Kinetics of long chain n-paraffin dehydrogenation over a commercial Pt-Sn-K-Mg/-Al2O3 catalyst

Model studies using n-dodecane

He, Songbo; Castello, Daniele; Krishnamurthy, K. R.; Al-Fatesh, Ahmed S.; Winkelman, J. G.M.; Seshan, K.; Fakeeha, Anis H.; Kersten, S. R.A.; Heeres, H. J.

Published in:
Applied Catalysis A: General

DOI (link to publication from Publisher):
10.1016/j.apcata.2019.04.026

Publication date:
2019

Document Version
Publisher's PDF, also known as Version of record

Applied Catalysis A, General 579 (2019) 130–140

Contents lists available at ScienceDirect

Applied Catalysis A, General

journal homepage: www.elsevier.com/locate/apcata

Kinetics of long chain *n*-paraffin dehydrogenation over a commercial Pt-Sn-K-Mg/γ-Al_2O_3 catalyst: Model studies using *n*-dodecane

Songbo He[a,b,*], Daniele Castello[b,c], K.R. Krishnamurthy[d], Ahmed S. Al-Fatesh[e], J.G.M. Winkelman[a], K. Seshan[b], Anis H. Fakeeha[e], S.R.A. Kersten[b], H.J. Heeres[a]

[a] Green Chemical Reaction Engineering, Engineering and Technology Institute Groningen, University of Groningen, 9747 AG, Groningen, The Netherlands
[b] Faculty of Science and Technology, University of Twente, 7500 AE, Enschede, The Netherlands
[c] Department of Energy Technology, Aalborg University, 9220, Aalborg Øst, Denmark
[d] National Centre for Catalysis Research, Indian Institute of Technology Madras, Chennai, 600036, India
[e] Chemical Engineering Department, College of Engineering, King Saud University, Riyadh 11421, Saudi Arabia

ARTICLE INFO

Keywords:
Dehydrogenation
Long chain paraffins
n-dodecane
Kinetic studies
Pt-Sn/Al_2O_3
Olefins

ABSTRACT

A kinetic modeling study on long chain *n*-paraffin dehydrogenation using a commercial Pt-Sn-K-Mg/γ-Al_2O_3 catalyst was carried out in a continuous flow set-up using *n*-dodecane as a model component at various temperatures (450-470 °C), pressures (0.17-0.30 MPa), H_2/paraffin mole ratios (3:1-6:1) and space times (0.22-1.57 g h mol^{-1}). The commercial catalyst was characterized by XRD, BET, MIP, SEM and CO chemisorption. An empirical exponential equation was found to predict the mono- and di-olefin yields very well. In addition, 6 mechanistic models based on the LHMW mechanism were derived and tested by non-linear least squares fitting of the experimental data. The model which assumes that surface reactions and particularly the dehydrogenation of the metal-alkyl chain to the adsorbed mono-olefin and di-olefin as the rate determining steps was found to give the best fit with the experimental data. In addition, activation energies and adsorption enthalpies for each elementary reaction were obtained. The kinetic testing and modeling have shown that the high mono-olefins selectivity for long chain paraffin dehydrogenation can be obtained by operating at low space time (when P, T and m are same), high pressure (when τ, T and m are same) and high H_2/paraffin ratio (when τ, P and T are same), as well as low reaction temperature (when τ, P and m are same) but with little effect.

1. Introduction

Dehydrogenation of long chain, kerosene range, *n*-paraffins to mono-olefins over a Pt-Sn/γ-Al_2O_3 based catalyst operated at high temperatures (475–490 °C) and low pressures (0.1 − 0.25 MPa) is an important step in the production of linear alkylbenzene sulfonates (LAS), with widespread applications as biodegradable detergents. The commercial feedstock is a mixture of *n*-paraffins with different chain lengths (generally *n*-C_{10}-C_{13}), each of which has a different dehydrogenation rate [1] and as such, the reaction network for *n*-paraffin dehydrogenation is very complicated. In addition, other reactions occur as well [2,3], examples are (i) cracking to lighter fractions, (ii) consecutive dehydrogenation and formation of aromatics *via* dehydrocyclization, and (iii) coke formation. These reactions take place on the metal and/or acid sites of the typically used bi-functional Pt-Sn/γ-Al_2O_3 catalysts. In order to obtain high mono-olefin selectivity, these side reactions forming dienes, trienes/aromatics [4,5], *etc.*, must be suppressed kinetically or inhibited by proper modification of the Pt-Sn/γ-Al_2O_3 catalyst. The high temperatures used for *n*-paraffin dehydrogenation to overcome thermodynamic equilibrium limitations also results in the formation of substantial amounts of coke. Modifications of the Pt-Sn/γ-Al_2O_3 catalyst by *e.g.*, the introduction of (i) alkaline [6–8], alkaline earth [9–11] and transition metals [12–14], (ii) rare earth elements [15], and (iii) the use of carbon as support [16,17], have been reported to improve the mono-olefin selectivity and catalyst life-time. Recently, a Pt-Sn-K-Mg/γ-Al_2O_3 catalyst has been commercialized in PetroChina, PR China [18], which is characterized by longer life-time (72 *vs.* 58 days), higher operation temperature (490 *vs.* 481 °C) and higher daily production (333.6 *vs.* 321.5 tons day^{-1}), as compared to Pt-Sn-K/γ-Al_2O_3 catalyst. The better performance of Pt-Sn-K-Mg/γ-Al_2O_3 catalyst was attributed to the higher mechanical strength and better thermal stability of Mg-Al-O support, as well as the moderated

* Corresponding author at: Green Chemical Reaction Engineering, Engineering and Technology Institute Groningen, University of Groningen, 9747 AG, Groningen, The Netherlands.
E-mail address: songbo.he@rug.nl (S. He).

https://doi.org/10.1016/j.apcata.2019.04.026
Received 19 February 2019; Received in revised form 18 April 2019; Accepted 19 April 2019
Available online 22 April 2019

Nomenclature

T	reaction temperature, °C
P	reaction pressure, Pa
X_P	conversion of paraffins, %
Y_O, Y_D	yield of mono-olefins and di-olefins, %
L	acid sites
M	Pt sites
K_2, K_3, K_5, K_6	equilibrium constants for reaction step *i*
K_P, K_O, K_{DM}, K_{DL}, K_{AM}, K_{AL},K_H	adsorption constants for paraffins, mono-olefins, di-olefins (on M and L sites), aromatics (on M and L sites) and H_2, Pa
k_1 - k_{11}	reaction rate constant for reaction step *i*, mol h^{-1} g^{-1} Pa^{-1}
r_P, r_O, r_D	rate of paraffins conversion, mono- and di-olefins formation, mol s^{-1} kg^{-1}
P_P, P_O, P_D, P_A, P_{H2}	partial pressure of paraffins, mono-olefins, di-olefins, aromatics and H_2, Pa
C_L, C_M	acid sites and Pt sites concentration, %
C_{PM}, C_{OM}, C_{DM}, C_{AM}, C_{HM}, C_{DL}, C_{AL}	concentration of paraffins, mono-olefins, di-olefins, aromatics and H adsorbed on Pt sites, and di-olefins, aromatics adsorbed on acid sites, %
C_{O1M}, C_{D1M}	concentration of half-dehydrogenated $C_{12}H_{25}$ and $C_{12}H_{23}$ adsorbed on Pt sites, %
W	catalyst weight, g
F_P	mole flow rate of paraffins, mol h^{-1}
τ	W/F_P = space time, kg s mol^{-1}
m	hydrogen/paraffin mole ratio

acidity, enhanced interaction of Pt and support, and the increased pore volume and pore size diameter resulted from adding Mg [9]. However, detailed kinetic studies on long chain paraffin dehydrogenation are scarce, although is of high importance for determining (i) the reaction mechanism, (ii) to establish reaction networks and (iii) to be used for reactor engineering studies, *e.g.*, for the proper simulation and design of commercial reactors.

Krylova et al. [19] investigated the kinetics of *n*-decane dehydrogenation over Pt-W-Li/Al_2O_3 catalyst using hydrogen/deuterium isotope exchange experiments and proposed a stepwise reaction scheme, in which the desorption of mono- and di-olefins was regarded as the rate determining step. This kinetic model was further expanded by Sadykhova et al. [20,21], and allowed determination of the kinetic parameters for *n*-decane, *n*-undecane and *n*-dodecane dehydrogenation over a Pt-Sn/Al_2O_3 catalyst. Basrur et al. [22] investigated the kinetics of *n*-decane dehydrogenation over the promoted Pt/Al_2O_3 catalyst using a Box-Wilson method and developed an empirical model for predicting paraffin conversion/olefin selectivity *vs.* operational parameters. Padmavathi et al. [23] studied the kinetics of *n*-dodecane dehydrogenation over a Pt-Sn-In-Fe-Li/Al_2O_3 catalyst and discriminated five possible reaction schemes using a Box optimization method. Their results indicate the occurrence of a stepwise mechanism for long chain paraffin dehydrogenation over such promoted Pt/Al_2O_3 catalysts. In addition, the most suitable kinetic model based on Langmuir–Hinshelwood–Hougen–Watson (LHHW) mechanism was determined in which the surface reaction was identified as the rate determining step. This kinetic scheme was further adopted by Vafajoo et al. [24] to optimize the rate parameters for commercial plant data by a Nelder-Mead (NM) simplex method. Ivashkina et al. [25] analyzed the thermodynamics of C_9-C_{14} dehydrogenation by means of quantum chemistry and established a kinetic model including deactivation due to coke formation. Kinetic models for deactivation of long chain paraffin dehydrogenation catalyst were also discussed by Gaidai et al. [26] and Saeedizad et al. [27]. It was shown [26,27] that coking was mainly caused by the formation of dienes. In previous studies by our group [28], it was found that three different types of coke were present at a deactivated Pt-Sn-K/Al_2O_3 catalyst used for long chain paraffin dehydrogenation. The coke was present at different positions on the catalytically active surface, *viz.* on Pt nanoparticle sites, acid sites on the Al_2O_3 support in close proximity of the Pt nanoparticles and discrete acid sites on the Al_2O_3 support.

It is generally accepted [29] that the dehydrogenation reactions (*e.g.*, dehydrogenation of paraffins and mono-olefins) are catalyzed by the metal (*e.g.*, Pt) sites of the bi-functional Pt-Sn/γ-Al_2O_3 catalyst whereas most of the side reactions (*e.g.*, isomerization and coking) take place on the Lewis acid sites of the catalyst. To the best of our knowledge, kinetic studies on long chain *n*-paraffin dehydrogenation considering both sites of the bi-functional Pt-Sn/γ-Al_2O_3 catalyst have not yet been considered, although it is highly relevant for designing an efficient catalyst with respect to mono-olefin selectivity and coking/catalyst deactivation. In this context a "bi-functional mechanistic model" is proposed for the first time. The kinetics of long chain *n*-paraffin dehydrogenation over an industrial Pt-Sn-K-Mg/γ-Al_2O_3 catalyst [18] using n-dodecane as the model component will be reported, applying LHHW mechanisms which were reported earlier [23,24] and commonly used for describing the catalytic dehydrogenation reactions [30]. The models include both surface reaction steps on metal nanoparticles (Pt) and acid sites. The best model was selected using appropriate model discrimination methods. Finally, relations to predict the mono- and di-olefin yield at different reaction conditions (temperature, pressure and H_2/paraffin ratio) were established and verified.

2. Experimental section

2.1. Materials

A recently commercialized Pt-Sn-K-Mg/γ-Al_2O_3 catalyst for long chain *n*-paraffin dehydrogenation [18], which contains 0.5 wt.% of Pt, 1.5 wt.% of Sn, 0.5 wt.% of K and 1.0 wt.% of Mg, produced at PetroChina Fushun Petrochemical Company, PR China, was used for this study. The γ-Al_2O_3 support was produced at the Research Institute of Daily Chemical Industry, PR China. The impregnation precursors, Pt, $SnCl_2$, HCl, KCl, $MgCl_2$ and ethanol, were of analytical grade (> 99.9% pure). The catalyst was prepared by wet impregnation (35 kg $batch^{-1}$) at 10^{-3} bar vacuum followed by drying at 70 °C (30 min), 120 °C (3 h) and calcination at 520 °C (8 h, 70 kg $batch^{-1}$). The catalyst was finally reduced under pure H_2 at 490 °C (8 h, 140 kg $batch^{-1}$). *n*-Dodecane (*n*-C_{12}°, 98.88 wt.%) was commercially supplied by Liaoyang HuiFu Chemical Factory, Liaoning, PR China. It contained minor amounts of *n*-C_{10}° (0.05 wt.%), *n*-C_{11}° (0.80 wt.%), *n*-C_{13}° (0.20 wt.%) and *n*-C_{14}° (0.07 wt.%).

2.2. Catalyst characterization

X-ray diffraction (XRD) spectra of the catalyst were obtained using a PAN Alytical X' Pert PRO instrument with Cu Kα radiation (40 kV and 40 mA) in the scan 2θ range of 20-80°.

The specific surface area of the catalyst was calculated from the adsorption isotherms obtained from nitrogen physisorption experiments at 77 K using a Micromeritics ASAP system (2010, USA) based on Brunauer-Emmett-Teller (BET) theory [31]. Pore size distributions (PSD) were calculated from the desorption branches of the isotherms according to the BJH (Barrett-Joyner-Halenda) method [32]. The catalyst was degassed at 300 °C prior to these measurements.

The total pore volume of the catalyst was measured using mercury intrusion porosimetry (MIP, Micromeritics Autopore 9520, USA). The catalyst was pre-degassed in vacuum (0.01 torr) for 1 h at 95 °C.

Scanning electron microscopy (SEM) measurements were performed

on a Quanta 200 (FEI Company) with an accelerating voltage of 20 kV.

Pt dispersion of the catalyst was determined by CO pulse chemisorption using a Micromeritics AutoChem II 2920 (USA). The catalyst was pre-reduced under pure H_2 (99.99%, 20 ml min^{-1}) at 500 °C for 1 h, purged with helium (99.99%, 20 ml min^{-1}) at 520 °C for 1 h and then cooled to 50 °C in He. 100 μL pulses of 5 vol.% CO/He were used and the time between pulses was 4 min. The adsorbed CO was determined by TCD and Pt dispersion calculations were based on the assumption that the value of CO/Pt_s is 1 [33].

2.3. Experimental setup and kinetic measurements

The experimental setup for *n*-dodecane dehydrogenation consisted of a micro-catalytic setup [34] with a fixed-bed reactor (tubular stainless steel, 10-mm-inner-diameter). The reactor was loaded with the commercial Pt-Sn-K-Mg/γ-Al_2O_3 catalyst (0.24 g), which was grounded to particle sizes between 0.25 − 0.6 mm to eliminate axial back-mixing and channeling effects in the catalyst bed. The catalyst was pre-reduced *in-situ* by hydrogen (99.995%, 500 ml min^{-1}) at 470 °C for 2 h. Reaction temperatures (T, 450, 460 and 470 °C) were measured by a thermocouple in the catalyst bed and used to control the reactor temperature by adjusting the electronic furnace temperature. Reactor pressures (P, 0.17, 0.24 and 0.30 MPa) were measured by a pressure gauge at the bottom of the catalyst bed and controlled by a back pressure regulator. *n*-Dodecane was fed to the reactor using an HPLC pump, and space times ($\tau = W/F_P$) between 0.22–1.57 $g_{catalyst}$ (mol $h^{-1})^{-1}$ were applied. The hydrogen flow was measured and controlled by mass flow controller and two hydrogen to paraffin mole ratios (m, 3:1 and 6:1) were applied. For each set of reaction conditions (*e.g.*, for each combination of T, P and m), 5 data points were collected by varying the space time (τ) over the catalyst. In total, 60 data points were collected for the modeling and an overview of the data is given in Table S1 (Supporting Information).

After reaction, the products and un-reacted paraffins were condensed and analyzed using an Agilent 7890 A (USA) Gas Chromatograph equipped with a flame ionization detector (FID) and an HP-FFAP column (30 m × 0.53 mm × 1.0 mm, Agilent, USA) [9]. The conversion of *n*-dodecane (X_P) was derived from its GC peak area percentage (A_P, Eq. 1). The selectivities (S) to mono- ($C_{12}^{=}$, S_O) and di-olefins ($C_{12}^{=\ =}$, S_D) were defined based on their fraction in the total products (Eq. 2). The corresponding yields (*Y*) were calculated using Eq. 3.

$$X_P = (1 - A_P) \times 100\%. \quad (1)$$

$$S_i = A_i/A_{total\ products}) \times 100\%.\ (_i \text{ represent } _O \text{ and } _D). \quad (2)$$

$$Y_i = X_p \times S_i\ (_i \text{ represent } _O \text{ and } _D). \quad (3)$$

2.4. Determination of external and internal diffusion limitations and heat transfer limitations

To study the effect of external diffusion on the kinetic data, two experiments were performed at 450 °C with different catalyst intakes (0.24 g and 0.48 g). The *n*-dodecane feed (F_P) and not the catalyst intake was varied to compare the *n*-dodecane conversion at equal space times ($\tau = W/F$) and the results are shown in Fig. 3. The curves for the *n*-dodecane conversion versus space time are similar for both catalyst intakes, implying that external diffusion effects are negligible when the space time is smaller than 1.5 g (mol $h^{-1})^{-1}$. Accordingly, the space time for all the kinetic experiments was below this value to eliminate external mass transport limitations.

The Weisz-Prater criterion (Eq. 4) was used to evaluate the relevance of internal diffusion effects.

$$N_{WP} = \frac{r_{P,obs} \times \rho_{cat} \times R_p^2}{C_P \times D_P} \quad (4)$$

where $r_{P,obs}$ is the observed average reaction rate of n-dodecane (mol kg^{-1} s^{-1}), ρ_{cat} is the density of the catalyst (kg m^{-3}), R_p is the average radius of the catalyst particles (m), C_P is the average concentration of n-dodecane (mol m^{-3}) and D_P is the internal diffusion of paraffin in the catalyst pores, assuming Knudsen diffusion (m^2 s^{-1}). Details on the calculation of the Weisz-Prater criterion are given in the Supplementary Information.

The calculated values of N_{WP} are shown in Table S1 for each experimental run. None of the experimental values exceeds 0.2, indicating the absence of internal diffusion limitation of *n*-dodecane. In addition, earlier experimental studies by us in the same reactor at similar reaction conditions as the present kinetic study with different catalyst particle sizes [34] also showed that internal diffusion effects were absent when using a catalyst with particle sizes in the range of 0.85–1.0 mm.

Possible internal heat transfer limitations were analyzed using the coupled concentration and temperature profiles inside the catalyst particles [35,36]. From the analysis, the calculated temperature differences inside the catalyst particles, $\Delta T_{particle} = T_{surface} - T_{center}$, were found as 0.03 K on average with a maximum value of 0.085 K (Table S1). These differences were considered too small to take into consideration.

Possible temperature differences due to external heat transfer limitations are quantified from a balance equating the rate of heat removal *via* the film with the rate of heat production in the catalyst particle. The results in the form of the calculated temperature differences over the film surrounding the catalyst particles, $\Delta T_{film} = T_g - T_{surace}$, are given in Table S1 and are on average 1.5 K with a maximum value of 3.85 K. These differences were considered too small to take into consideration as well.

3. Kinetic modeling and parameter fitting for n-dodecane dehydrogenation

3.1. Reaction schemes and assumptions

Two major reaction pathways have been established for long chain paraffin dehydrogenation [2,3,37]. On an un-modified Pt/Al_2O_3 catalyst, the reaction network involves consecutive dehydrogenations to form *n*-olefins, *n*-dienes and *n*-trienes followed by dehydrocyclization to form aromatics (RP1) [2,3,29].

Paraffins ↔ mono-olefins ↔ di-olefins ↔ tri-olefins → aromatics(RP1)

In parallel, isomerization, dehydrocyclization (of paraffins), cracking and coking also take place. The latter pathway is particularly catalyzed by the acid sites of the catalyst. When the acidity of the catalyst is reduced (*e.g.*, by alkali doping), the latter pathway is suppressed.

When using modified catalysts (Pt-Sn-K-Mg/γ-Al_2O_3 catalyst, [5]), as in this study, tri-olefins at any given time were too low for detection, in line with the observation from the industrial long chain paraffin process and the analysis of reaction products using temperature-programmed reaction/single-photon ionization time-of-flight mass spectrometry (TPRn/SPI-TOF-MS) measurements [4,5], which is likely due to that they are the transient species and get converted at a very fast rate to aromatics. As such, tri-olefins are not considered in the model. Accordingly, the consecutive reaction pathway (RP1) can be simplified to RP2.

$$\text{Paraffins} \overset{r_P}{\leftrightarrow} \text{mono-olefins} \overset{r_O}{\leftrightarrow} \text{di-olefins} \overset{r_D}{\rightarrow} \text{aromatics} \quad \text{(RP2)}$$

Langmuir - Hinshelwood - Hougen - Watson (LHHW) and Power - Law (P-L) models are commonly used in heterogeneous catalysis. Padmavathi et al. [23] and Vafjoo et al. [24] have shown that LHHW

based models fitted the experimental data well, though without specifying catalytic sites. We here consider two types of adsorption sites on the bi-functional Pt-Sn/γ-Al_2O_3 based catalyst, *viz.*, metal nanoparticle sites (Pt, denoted as M) and Lewis acid sites (denoted as L). The proposed reaction scheme consists of 13 reactions, including adsorption/desorption equilibria and surface reactions (Table 1). All reactions were considered to be reversible, elementary reactions, the only exceptions being dehydrogenation of adsorbed di-olefins on M sites (Reaction No. 8 in Table 1) and for the formation of aromatics from adsorbed di-olefins on L sites cooperated with M sites (Reaction No. 11 in Table 1). These two reactions were considered as irreversible [2,3] as thermodynamically most stable product, *viz.*, aromatics, is formed and the backward reactions are expected to occur with very low rates. The reaction scheme is summarized in Scheme 1 and was set up using the following assumptions (H1-H10).

H1. Existence of three different active sites [28], *viz.*, Pt nanoparticles, Al_2O_3 support acid sites with Pt naoparticles in close vicinity and isolated acid sites on the Al_2O_3 support. As experimental techniques allow only to measure the total number of Lewis acid sites and it is not possible to estimate the fraction of the above two types of acid sites, they are lumped as Lewis acid sites to simplify the kinetic model. The Lewis acid sites of interest are a fixed fraction because there is only one catalyst being used, it will be incorporated in the rate constants for the steps where the Lewis acid sites are involved.

H2. The paraffins, mono-olefins and di-olefins react on Pt sites according to reaction sequence RP2 [5].

H3. Adsorption of paraffins occurs only on the Pt sites.

H4. Dehydrogenation of paraffins on Pt sites proceeds step-wise, *viz.*, first formation of adsorbed M-alkyl and M−H species. In the next step, the M-alkyl species react to yield an adsorbed mono-olefin and a second M−H species.

H5. Hydrogen gas is formed by a surface reaction between two adsorbed M−H species on Pt sites [23,30].

H6. The adsorbed mono-olefins, di-olefins, aromatics and H_2 species on Pt sites can be desorbed to form the corresponding products.

H7. The desorbed di-olefins can also be adsorbed on the Lewis acid sites. The desorbed mono-olefins from metal sites was not considered to re-adsorb on Lewis acid sites due to the adsorption on Lewis acid sites is always weaker than metal sites and minor. And practically, the catalyst design and reaction conditions (*e.g.*, low contact time) for long chain paraffin dehydrogenation are optimized to render the mono-olefins desorption a facile process.

H8. The adsorbed di-olefins on Lewis acid sites can be transformed into aromatics *via* dehydrocyclization in cooperation of Pt sites [29] follows step-wise reaction mechanisms. These stepwise reactions are lumped in one reaction to simplify the model, due to the fact that dehydrocyclization is not the core reaction and minimized in long chain paraffin dehydrogenation process.

H9. The adsorbed aromatics on the Lewis acid sites can be desorbed to form aromatics.

H10. Coking and cracking reactions are not included in the model. This is due to the fact that their reaction rates are so low that the corresponding products are not detectable at the reaction conditions applied. This can also be indicated by the reported long life-time of and low coke deposition on the catalysts for long chain *n*-paraffins dehydrogenation, which were 30 days and 8 wt.% for Pt-Sn-Li/Al_2O_3 [38], 37 days and 7.9 wt.% for Pt-Sn-In-Fe/Al_2O_3 [39], and 72 days and 3.8 wt.% for the Pt-Sn-K-Mg/γ-Al_2O_3 catalyst investigated in this kinetic study [18].

3.2. From reaction network to kinetic models

To obtain expressions for the three reaction rates r_P, r_O and r_D (RP2), the Langmuir-Hinshelwood-Hougen-Watson (LHHW) approach was followed, assuming that certain reactions among those presented in Table 1 are rate determining (rds). A total of 6 different kinetic models were derived:

3.2.1. Model 1: Adsorption of paraffins (reaction 1 in Table 1) is rate determining

$$r_P = k'_P \frac{K_P P_P - \frac{K_{DM} P_D}{K_2}(K_H P_{H_2})^2}{DEN}$$

$$r_O = k'_O \frac{K_O P_O - \frac{K_{DM} P_D}{K_5 K_6} K_H P_{H_2}}{DEN}$$

$$r_D = k'_{DM} \frac{K_{DM} P_D}{DEN^5} + k'_{DL} \frac{K_{DL} P_D}{(1 + K_{DL} P_D + K_{AL} P_A) DEN^4}$$

Table 1
Reaction schemes for *n*-dodecane dehydrogenation over Pt-Sn-K-Mg/γ-Al_2O_3 catalyst.

Reaction steps	Elementary reaction	Reaction rate	Equilibrium constant
1. Paraffins adsorption on M sites	$C_{12}H_{26} + M \leftrightarrow C_{12}H_{26}M$	$k_1(P_P C_M - \frac{1}{K_P} C_{PM})$	$K_P = \frac{C_{PM}}{P_P C_M}$
2. Dehydrogenation of adsorbed paraffins on M sites – 1st step	$C_{12}H_{26}M + M \leftrightarrow C_{12}H_{25}M + HM$	$k_2(C_{PM} C_M - \frac{1}{K_2} C_{O1M} C_{HM})$	$K_2 = \frac{C_{O1M} C_{HM}}{C_{PM} C_M}$
3. Dehydrogenation of adsorbed paraffins on M sites – 2nd step	$C_{12}H_{25}M + M \leftrightarrow C_{12}H_{24}M + HM$	$k_3(C_{O1M} C_M - \frac{1}{K_3} C_{OM} C_{HM})$	$K_3 = \frac{C_{OM} C_{HM}}{C_{O1M} C_M}$
4. Mono-olefins desorption	$C_{12}H_{24}M \leftrightarrow C_{12}H_{24} + M$	$k_4(C_{OM} - K_O P_O C_M)$	$K_O = \frac{C_{OM}}{P_O C_M}$
5. Dehydrogenation of adsorbed mono-olefins on M sites – 1st step	$C_{12}H_{24}M + M \leftrightarrow C_{12}H_{23}M + HM$	$k_5(C_{OM} C_M - \frac{1}{K_5} C_{D1M} C_{HM})$	$K_5 = \frac{C_{D1M} C_{HM}}{C_{OM} C_M}$
6. Dehydrogenation of adsorbed mono-olefins on M sites – 2nd step	$C_{12}H_{23}M + M \leftrightarrow C_{12}H_{22}M + HM$	$k_6(C_{D1M} C_M - \frac{1}{K_6} C_{DM} C_{HM})$	$K_6 = \frac{C_{DM} C_{HM}}{C_{D1M} C_M}$
7. Di-olefins desorption	$C_{12}H_{22}M \leftrightarrow C_{12}H_{22} + M$	$k_7(C_{DM} - K_{DM} P_D C_M)$	$K_{DM} = \frac{C_{DM}}{P_D C_M}$
8. Dehydrogenation of adsorbed di-olefins on M sites	$C_{12}H_{22}M + 4M \rightarrow C_{12}H_{18}M + 4HM$	$k_8 C_{DM} C_M^4$	*(non-equilibrium)*
9. Di-olefins adsorption on L site	$C_{12}H_{22} + L \leftrightarrow C_{12}H_{22}L$	$k_9(P_D C_L - \frac{1}{K_{DL}} C_{DL})$	$K_{DL} = \frac{C_{DL}}{P_D C_L}$
10. Aromatics desorption from M site	$C_{12}H_{18}M \leftrightarrow C_{12}H_{18} + M$	$k_{10}(C_{AM} - K_{AM} P_A C_M)$	$K_{AM} = \frac{C_{AM}}{P_A C_M}$
11. Aromatics formation from adsorbed di-olefins on L sites cooperated with M sites	$C_{12}H_{22}L + 4M \rightarrow C_{12}H_{18}L + 4HM$	$k_{11} C_{DL} C_M^4$	*(non-equilibrium)*
12. Aromatics desorption from L sites	$C_{12}H_{18}L \leftrightarrow C_{12}H_{18} + L$	$k_{12}(C_{AL} - K_{AL} P_A C_L)$	$K_{AL} = \frac{C_{AL}}{P_A C_L}$
13. Hydrogen gas formation	$2HM \leftrightarrow H_2 + 2M$	$k_{13}(C_{HM}^2 - K_H P_{H_2} C_M^2)$	$K_H = \frac{C_{HM}^2}{P_{H_2} C_M^2}$

L: Lewis acid sites; M: Pt sites.

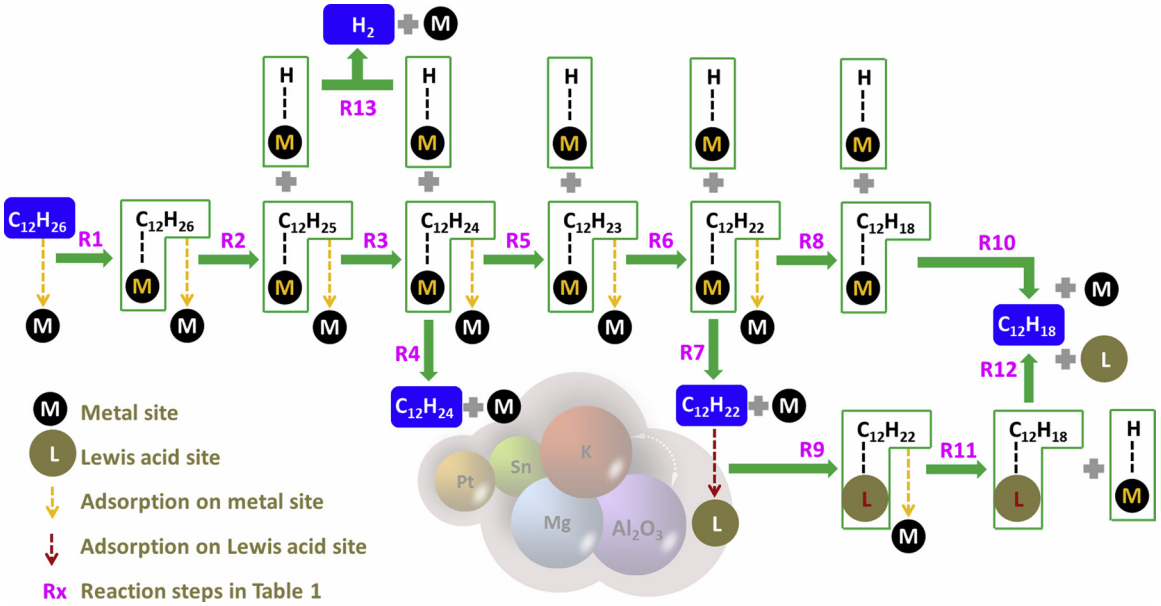

Scheme 1. Reaction schemes for *n*-dodecane dehydrogenation over Pt-Sn-K-Mg/γ-Al_2O_3 catalyst.

$$DEN = 1 + \frac{K_{DM}P_D}{K_2K_3K_5K_6}(K_HP_{H_2})^2 + \frac{K_{DM}P_D}{K_3K_5K_6}(K_HP_{H_2})^{1.5} + \frac{K_{DM}P_D}{K_5K_6}(K_HP_{H_2}) + \frac{K_{DM}P_D}{K_6}(K_HP_{H_2})^{0.5} + K_{DM}P_D + K_{AM}P_A + (K_HP_{H_2})^{0.5}$$

3.2.2. Model 2: Dehydrogenations of absorbed paraffins and mono-olefins (surface reactions 2 and 5 in Table 1) are the rds

$$r_P = k'_P\frac{K_PP_P - \frac{K_OP_O}{K_2K_3}K_HP_{H_2}}{DEN^2}$$

$$r_O = k'_O\frac{K_OP_O - \frac{K_{DM}P_D}{K_5K_6}K_HP_{H_2}}{DEN^2}$$

$$r_D = k'_{DM}\frac{K_{DM}P_D}{DEN^5} + k'_{DL}\frac{K_{DL}P_D}{(1 + K_{DL}P_D + K_{AL}P_A)DEN^4}$$

$$DEN = 1 + K_PP_P + \frac{K_OP_O}{K_3}(K_HP_{H_2})^{0.5} + K_OP_O + \frac{K_{DM}P_D}{K_6}(K_HP_{H_2})^{0.5} + K_{DM}P_D + K_{AM}P_A + (K_HP_{H_2})^{0.5}$$

3.2.3. Model 3: Dehydrogenations of absorbed paraffins and mono-olefins (surface reactions 3 and 5 in Table 1) are the rds

$$r_P = k'_P\frac{K_2K_PP_P(K_HP_{H_2})^{-0.5} - \frac{K_OP_O}{K_3}(K_HP_{H_2})^{0.5}}{DEN^2}$$

$$r_O = k'_O\frac{K_OP_O - \frac{K_{DM}P_D}{K_5K_6}K_HP_{H_2}}{DEN^2}$$

$$r_D = k'_{DM}\frac{K_{DM}P_D}{DEN^5} + k'_{DL}\frac{K_{DL}P_D}{(1 + K_{DL}P_D + K_{AL}P_A)DEN^4}$$

$$DEN = 1 + K_PP_P + K_2K_PP_P(K_HP_{H_2})^{-0.5} + K_OP_O + \frac{K_{DM}P_D}{K_6}(K_HP_{H_2})^{0.5} + K_{DM}P_D + K_{AM}P_A + (K_HP_{H_2})^{0.5}$$

3.2.4. Model 4: Dehydrogenations of absorbed paraffins and mono-olefins (surface reactions 2 and 6 in Table 1) are the rds

$$r_P = k'_P\frac{K_PP_P - \frac{K_OP_O}{K_2K_3}K_HP_{H_2}}{DEN^2}$$

$$r_O = k'_O\frac{K_5K_OP_O(K_HP_{H_2})^{-0.5} - \frac{K_{DM}P_D}{K_6}(K_HP_{H_2})^{0.5}}{DEN^2}$$

$$r_D = k'_{DM}\frac{K_{DM}P_D}{DEN^5} + k'_{DL}\frac{K_{DL}P_D}{(1 + K_{DL}P_D + K_{AL}P_A)DEN^4}$$

$$DEN = 1 + K_PP_P + \frac{K_OP_O}{K_3}(K_HP_{H_2})^{0.5} + K_OP_O + K_5K_OP_O(K_HP_{H_2})^{-0.5} + K_{DM}P_D + K_{AM}P_A + (K_HP_{H_2})^{0.5}$$

3.2.5. Model 5: Dehydrogenations of absorbed paraffins and mono-olefins (surface reactions 3 and 6 in Table 1) are the rds

$$r_P = k'_P\frac{K_2K_PP_P(K_HP_{H_2})^{-0.5} - \frac{K_OP_O}{K_3}(K_HP_{H_2})^{0.5}}{DEN^2}$$

$$r_O = k'_O\frac{K_5K_OP_O(K_HP_{H_2})^{-0.5} - \frac{K_{DM}P_D}{K_6}(K_HP_{H_2})^{0.5}}{DEN^2}$$

$$r_D = k'_{DM}\frac{K_{DM}P_D}{DEN^5} + k'_{DL}\frac{K_{DL}P_D}{(1 + K_{DL}P_D + K_{AL}P_A)DEN^4}$$

$$DEN = 1 + K_PP_P + K_2K_PP_P(K_HP_{H_2})^{-0.5} + K_OP_O + K_5K_OP_O(K_HP_{H_2})^{-0.5} + K_{DM}P_D + K_{AM}P_A + (K_HP_{H_2})^{0.5}$$

3.2.6. Model 6: Desorption of mono-olefins and di-olefins (reactions 4 and 7 in Table 1) are the rds

$$r_P = k'_P\frac{K_2K_3K_PP_P(K_HP_{H_2})^{-1} - K_OP_O}{DEN}$$

$$r_O = k'_O\frac{K_2K_3K_5K_6K_PP_P(K_HP_{H_2})^{-2} - K_{DM}P_D}{DEN}$$

$$r_D = k'_{DM}\frac{K_2K_3K_5K_6K_PP_P(K_HP_{H_2})^{-2}}{DEN^5} + k'_{DL}\frac{K_{DL}P_D}{(1 + K_{DL}P_D + K_{AL}P_A)DEN^4}$$

$$DEN = 1 + K_P P_P + K_2 K_P P_P (K_H P_{H_2})^{-0.5} + K_2 K_3 K_P P_P (K_H P_{H_2})^{-1} + K_2 K_3 K_5 K_P P_P (K_H P_{H_2})^{-1.5} + K_2 K_3 K_5 K_6 K_P P_P (K_H P_{H_2})^{-2} + K_{AM} P_A + (K_H P_{H_2})^{0.5}$$

The dependency of kinetic parameters and equilibrium constants on temperature can be indicated by Arrhenius equation (Eq. 5) and Van 't Hoff equation (Eq. 6), separately.

$$k_i = k_{0,i} \times \exp(-\frac{Ea_i}{RT}) \quad (5)$$

$$K_i = K_{0,i} \times \exp(-\frac{\Delta H_i}{RT}) \quad (6)$$

Hence, for each parameter stated in the formulae above, two kinetic constants were estimated, *viz.,* the pre-exponential factor ($k_{0,i}$ or $K_{0,i}$) and the activation energy (Ea_i) or enthalpy (ΔH_i). Most parameters were imposed to be positive, in order to be physically meaningful. However, the enthalpy of adsorption reactions (*e.g.,* for reactions No. 1, 4, 7, 10 and 12, Table 1) were set to be negative because adsorption is an exothermic process.

3.3. Reactor modeling and parameter estimation

The reactions were carried out in a fixed bed reactor and it was assumed that the reactor behaves as a PFR reactor. Volume expansion in the reactor was not considered as it is limited due to the low conversion of *n*-dodecane (*e.g.*, < 10%) and very high amount of hydrogen gas (*e.g.*, H_2/paraffin mole ratios was 3:1 - 6:1) was used as the dilution gas. As such, the following 5 ordinary differential equations (ODEs, Eqs. 7–11) were used for reactor modeling.

$$\frac{dP_P}{d\tau} = -P_T r_P \quad (7)$$

$$\frac{dP_O}{d\tau} = P_T (r_P - r_O) \quad (8)$$

$$\frac{dP_D}{d\tau} = P_T (r_O - r_D) \quad (9)$$

$$\frac{dP_A}{d\tau} = P_T r_D \quad (10)$$

$$\frac{dP_{H2}}{d\tau} = P_T (r_P + r_D + 2r_D) \quad (11)$$

where P_T is the total pressure and τ is the space time. The initial conditions are represented by the initial partial pressures of n-dodecane and hydrogen, which can be calculated from the experimental pressure and the hydrogen to paraffin ratio in the feed (m). By integrating the system between 0 and the desired space time τ, it is possible to determine the partial pressures of all the species involved. Eqs. 7–11 were implemented in the software package Matlab™ (The Mathworks, Inc.) and solved using the function ode15 s.

Parameter estimation was performed in MatLab™ using the function lsqnonlin, which is based on a non-linear least square minimization method and involved all 60 experimentally obtained data points (Table S1). The sum of the normalized squared deviations (NSD) was optimized. For the i^{th} species and the j^{th} experiment, the normalized deviation $NSD_{i,j}$ is defined as Eq. 12.

$$NSD_{i,j} = \left(\frac{X_{i,j}^{mod} - X_{i,j}^{exp}}{X_{i,max}^{exp}} \right)^2 \quad (12)$$

where x is the conversion (for paraffins) or yield (for mono-olefins and di-olefins) for model and experiments. The use of normalized deviations was preferred over relative errors as the latter method gives an excessive weight to the smaller values, resulting in a poor fitting for the higher ones.

For model discrimination, the root mean squared error (RMSE) and the Pearson's correlation coefficient R^2 for each model were calculated for each species.

4. Results and discussions

4.1. Characteristics of the industrial Pt-Sn-K-Mg/γ-Al2O3 catalyst

The Pt-Sn-K-Mg/γ-Al_2O_3 catalyst was characterised using XRD, nitrogen physisorption, mercury intrusion porosimetry (MIP) and SEM and the results are shown in Fig. 1 and summarised in Table 2. XRD patterns of the catalyst (Fig. 1a) show h-k-l reflections characteristic of the γ-Al_2O_3 phase (JCPD No. 04-0858). The nitrogen adsorption/desorption data (Fig. 1b) of the catalyst show a type IV isotherm and a H1-type hysteresis loop [40], indicating the presence of mesoporous and macroporous cylindrical pores. This is further illustrated by the PSD obtained by the BJH method (Fig. 1b) and the MIP data (Fig. 1c). The bimodal PSD structure (Fig. 1c, centered at 14.6 nm and 1300 nm) is typical for long chain paraffin dehydrogenation catalysts.

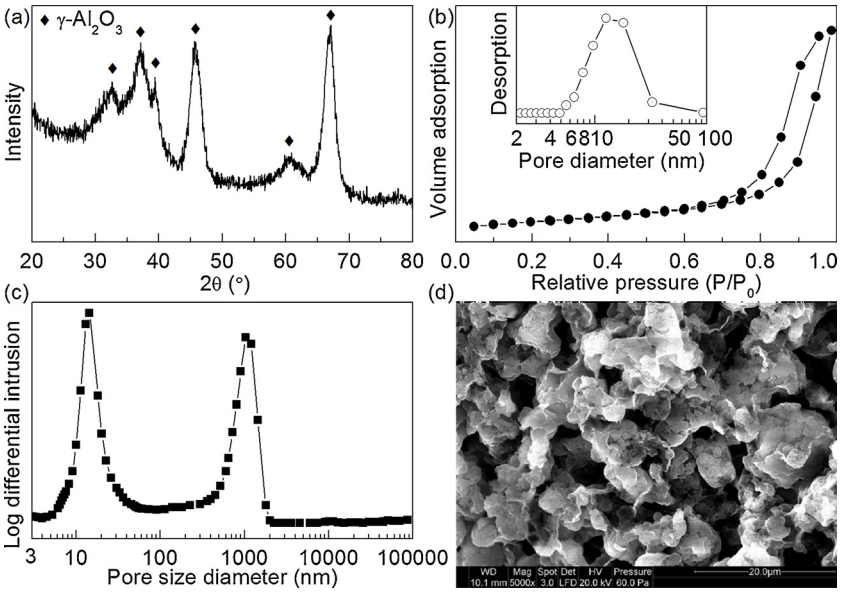

Fig. 1. (a) XRD, (b) BET, (c) MIP and (d) SEM of Pt-Sn-K-Mg/γ-Al_2O_3 catalyst.

Table 2
Characteristics of the Pt-Sn-K-Mg/γ-Al_2O_3 catalyst used in this study.

Catalysts	Shape	Bulk density (g cm^{-3})	$S_{BET}(N_2)$ ($m^2 g^{-1}$)	Pore volume ($cm^3 g^{-1}$)	Pt dispersion (%)
$Pt_{0.5}$-$Sn_{1.5}$-$K_{0.5}$-$Mg_{1.0}$/γ-Al_2O_3[a]	Granule, φ1.25 – 2.5 mm	0.33	149	1.46	70

[a] nominal metal loading, wt.%.

4.2. Effect of the process conditions on n-dodecane dehydrogenation

The yields of mono-olefins and di-olefins during *n*-dodecane dehydrogenation over Pt-Sn-K-Mg/γ-Al_2O_3 catalyst at different temperatures (T), pressures (P), H_2/paraffin ratios (m) and space times (τ) are plotted in Fig. 2. It can be seen from Fig. 2 that when P, m and τ are constant (*e.g.*, P = 0.24 MPa, m = 6:1 and τ = 0.45), higher reaction temperature leads to an increase in the yields of mono-olefin (Y_O, Fig. 2a, c and e) and di-olefin (Y_D, Fig. 2b, d and f). When T, m and τ are the same (*e.g.*, T = 450 °C, m = 6:1 and τ = 0.45), increasing the reaction pressure decreases the yields of mono-olefin (Y_O, Fig. 2a) and di-olefin (Y_D, Fig. 2b). When T, P and τ are same (*e.g.*, T = 460 °C, P = 0.17 MPa and τ = 0.45), increasing the H_2/paraffin ratio (m) lowers the yields of mono-olefin (Y_O, Fig. 2c) and di-olefin (Y_D, Fig. 2d). When T, P and m are constant (*e.g.*, T = 470 °C, P = 0.30 MPa and m = 6:1), increasing the space time (τ) over the catalyst favors higher yields of mono-olefin (Y_O, Fig. 2e) and di-olefin (Y_D, Fig. 2f). These trends follow from the thermodynamics of dehydrogenation of long chain paraffins to olefins, which is an endothermic reversible reaction accompanied by volume expansion.

The effect of the space time (τ) and yields of mono- and di-olefins (Y_O and Y_D) was modeled using a simple empirical approach (Eq. 13).

$$Y = -A \times exp + \left(\frac{-\tau}{B}\right) C \tag{13}$$

The results are shown in Fig. 2 (solid lines) and the equations with parameter values are given in the Supplementary Information. Agreement between the experimental data and the predicted values is very good. The Empirical modeling (Eqs. 13, S1 and S2) and our kinetic testing (Fig. 2) reveal that the increased selectivity of mono-olefins (or the ratio of mono-olefins yields to di-olefins yields) can be obtained by operating at low space time (when P, T and m are same), low reaction temperature (when τ, P and m are same), high pressure (when τ, T and m are same) and high H_2/paraffin ratio (when τ, P and T are same).

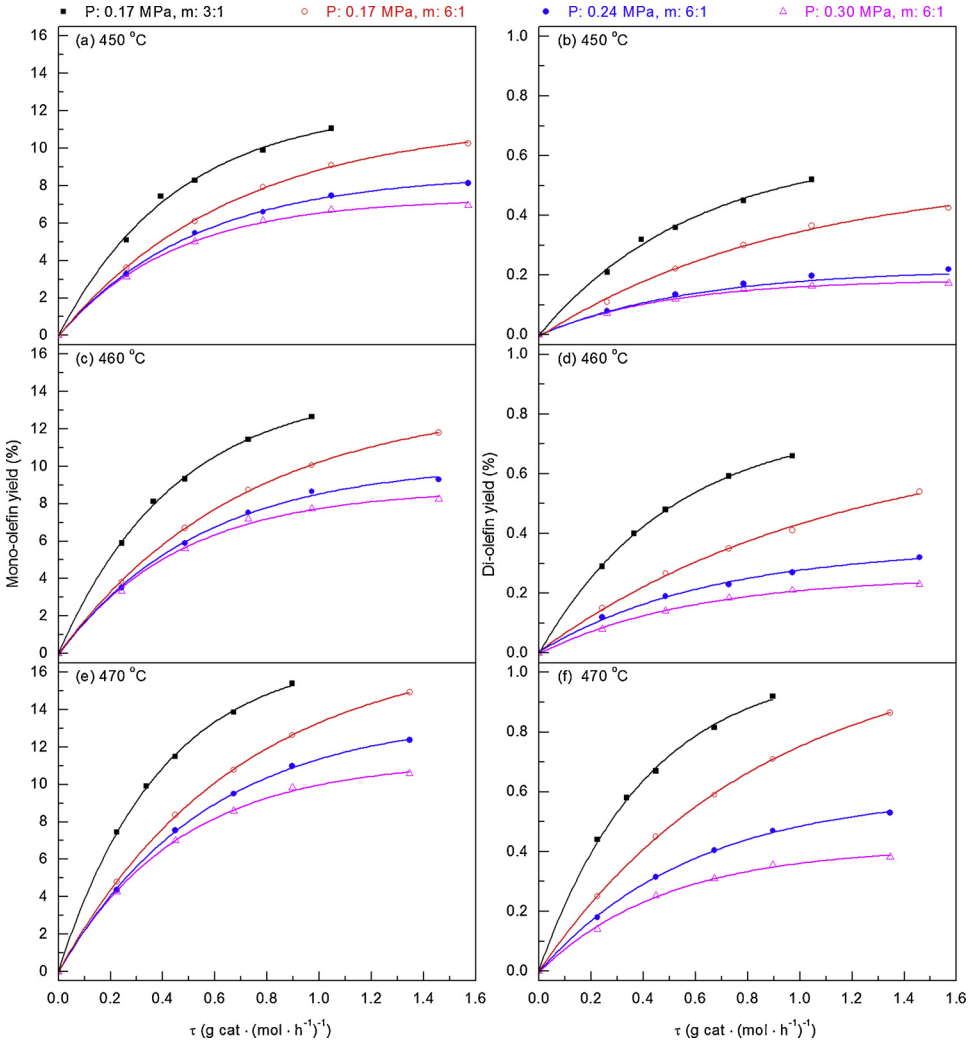

Fig. 2. Mono-olefin and di-olefin yield for *n*-dodecane dehydrogenation over Pt-Sn-K-Mg/γ-Al_2O_3 catalyst at different reaction conditions.

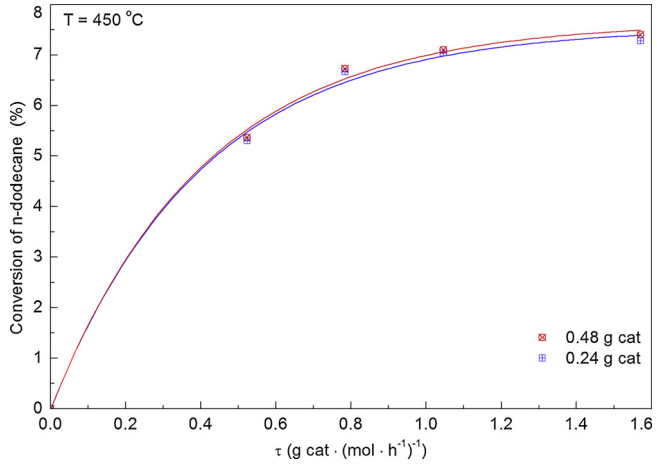

Fig. 3. Influence of space time on conversion of *n*-dodecane dehydrogenation over Pt-Sn-K-Mg/γ-Al_2O_3 catalyst.

4.3. Kinetic modelling results

The experimental data set with 60 experiments at a range of conditions was used for kinetic modeling. The model quality indicators (NSD, RMSE and R^2) for the 6 different models tested are provided in Table 3 whereas the corresponding kinetic parameters for each model are given in Table 4. The models based on adsorption (Model 1) and desorption (Model 6) as the rds show significantly higher values for the NSD and RMSE and lower values for R^2 than the models based on surface reactions (Models 2–5). As such, models with surface reactions as the rate determining steps seem to fit the experimental data better, which is consistent with previous research [23]. This is also supported by considering the parity plots in Fig. 4 and Figs. S2–S5.

At first sight, the model quality indicators for the remaining four models with surface reactions as the rds are rather similar (Table 3). However, Model 4 and 5 present slightly lower values for the RMSE and NSD compared to the other two surface-reaction-based models (Models 2 and 3). Both Models 4 and 5 assume that the rds is the dehydrogenation of half-dehydrogenated $C_{12}H_{23}M$ species adsorbed on Pt sites to the adsorbed di-olefin, *viz.*, the second step of mono-olefin dehydrogenation to di-olefin (Reaction 6, Table 1). These findings imply that the second step of mono-olefin dehydrogenation is slower than the first.

The activation energies of Model 4 (54.5 KJ mol^{-1}) and Model 5 (59.3 KJ mol^{-1}) for dodecane dehydrogenation to mono-olefins are in the range (31.4–78.0 KJ mol^{-1}) reported for dodecane dehydrogenation by Sadykhova et al. [21], Kang et al. [41], Padmavathi et al. [23] and Jiang et al. [42]. Further detailed comparison between Models 4 and 5 show that the Pearson's correlation coefficient for Model 5 is better than for Model 4, in line with the parity plots in Fig. 4. Thus Model 5 was selected as the best model for this kinetic study, which assumed that the rate determining steps are represented by the second step in the dehydrogenation of both paraffin and mono-olefin (r_P and r_O).

The activation energies of Model 5 for dodecane dehydrogenation to mono-olefins (59.3 KJ mol^{-1}) and for mono-olefins dehydrogenation to di-olefins (53.9 KJ mol^{-1}) are very close, indicating the formation of mono-olefins and di-olefins have similar sensitivity with the temperature increase. This is also well reflected by the small change of mono-olefins to di-olefins ratio when the temperature increases from 450 °C to 470 °C during the kinetic testing. Practically, we have also observed that the selectivity of mono-olefins is relatively stable (or slightly decreased) during the life-span of 72 days when the operation temperature in the industrial plant increases from 478 °C to 490 °C to keep the productivity [18]. This can be kinetically explained from our kinetic modeling which proves that the increase of temperature (*e.g.*, 450–490 °C) has little effect on mono-olefins to di-olefins ratio related to their similar reaction activation energy. As such, other operation parameters, *e.g.*, pressure, should be resorted to more effectively tune the mono-olefin selectivity for long chain paraffins dehydrogenation, indicated by the above kinetic testing and modeling.

A previous mechanistic study [29] has shown that the metal sites are required to cleave the C–H bond of the adsorbed paraffin (or mono-olefin). Only when the two neighboring C atoms are activated, the corresponding mono-olefin (or di-olefin) can be formed (RP3). The present kinetic results reveal that the half-dehydrogenated paraffin and mono-olefin adsorbed on the metal sites are more difficult to be dehydrogenated (Step 2, Reactions No. 3 and 6, Table 1) on the neighboring metal sites than the first step (dehydrogenation of the paraffin and mono-olefin adsorbed on the metal sites, Reactions No. 2 and 5, Table 1). This is due to the fact that the second dehydrogenation step requires extra metal sites which are present and adjacent to those adsorbing the half-dehydrogenated species. Thus lowering the liquid hourly space velocity (LHSV) of paraffins (*viz.*, increasing τ) while keeping T, P and m same can decrease the concentration of the adsorbed paraffin (or mono-olefins) on metal sites (*e.g.*, Pt) surface, leading to the increased yields of mono-olefins and di-olefins which is in line with the observation from our kinetic testing (Fig. 2). Alternatively, increasing the loading of the noble metal (*e.g.*, Pt) on the long chain paraffin dehydrogenation catalyst might be another option to increase the overall reaction rate. However, it was often observed that increasing Pt loading decreases the Pt dispersion [43], resulting in a lowering of the rate of olefin formation [44]. Our kinetic results also indicates that the noble metals (*e.g.*, Pt) are not required in large quantities but are needed to be highly dispersed on the support (*e.g.*, γ-Al_2O_3 with high surface area) [2] to generate high concentration of Pt particle surface per support surface area.

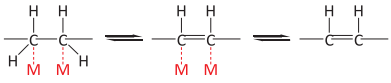

(RP3)

It is interesting to notice that the reaction rate for the aromatization step (Table 1) for the best model (Model 5) includes two additive terms. One involves K_{DL} which takes into account the synergy between Pt and acid sites (Reaction 11, Table 1) and the other one is K_{DM}, where the

Table 3
Model quality indicators for the 6 kinetic models.

Reaction model	Normalized squared deviation (NSD)	Root of mean squared error (RMSE)				Pearson's correlation coefficient (R^2)			
		P[a]	O[b]	D[c]	average	P[a]	O[b]	D[c]	average
Model 1	0.3392	0.0612	0.1388	0.1611	0.1203	0.9701	0.9534	0.9639	0.9625
Model 2	0.2257	0.0726	0.0890	0.1121	0.0912	0.9750	0.9737	0.9715	0.9734
Model 3	0.2591	0.0623	0.1149	0.1229	0.1000	0.9660	0.9670	0.9712	0.9681
Model 4	0.2218	0.0795	0.0631	0.1007	0.0811	0.9423	0.9826	0.9789	0.9679
Model 5	0.2213	0.0881	0.0615	0.0968	0.0821	0.9709	0.9800	0.9727	0.9745
Model 6	1.0703	0.1497	0.0806	0.2684	0.1662	0.9612	0.9509	0.8021	0.9047

P[a]: paraffins; O[b]: mono-olefins; D[c]: di-olefins.

Table 4
Reaction rate constants, reaction equilibrium constants and adsorption constants for *n*-dodecane dehydrogenation over Pt-Sn-K-Mg/γ-Al_2O_3 catalysts. The values of activation energy are given in kJ mol^{-1}.

Model 1	Model 2	Model 3	Model 4	Model 5	Model 6
$K_P = 2.4E\text{-}4 \times \exp\left(\frac{1.1}{RT}\right)$ Pa^{-1}	$K_P = 1.4E\text{-}5 \times \exp\left(\frac{0.8}{RT}\right)$ Pa^{-1}	$K_P = 4.1E\text{-}6 \times \exp\left(\frac{1.0}{RT}\right)$ Pa^{-1}	$K_P = 2.0E\text{-}7 \times \exp\left(\frac{0.9}{RT}\right)$ Pa^{-1}	$K_P = 2.1E\text{-}6 \times \exp\left(\frac{1.0}{RT}\right)$ Pa^{-1}	$K_P = 1.8E\text{-}4 \times \exp\left(\frac{1.0}{RT}\right)$ Pa^{-1}
$K_2 = 2.9E1 \times \exp\left(-\frac{27.3}{RT}\right)$	$K_2 = 5.9E2 \times \exp\left(-\frac{25.5}{RT}\right)$	$K_2 = 4.5E2 \times \exp\left(-\frac{26.2}{RT}\right)$	$K_2 = 4.7E2 \times \exp\left(-\frac{28.4}{RT}\right)$	$K_2 = 1.9E2 \times \exp\left(-\frac{26.2}{RT}\right)$	$K_2 = 3.1E1 \times \exp\left(-\frac{21.3}{RT}\right)$
$K_3 = 3.1E2 \times \exp\left(-\frac{22.4}{RT}\right)$	$K_3 = 1.0E2 \times \exp\left(-\frac{35.0}{RT}\right)$	$K_3 = 1.0E2 \times \exp\left(-\frac{36.8}{RT}\right)$	$K_3 = 4.2E2 \times \exp\left(-\frac{26.1}{RT}\right)$	$K_3 = 1.4E2 \times \exp\left(-\frac{33.1}{RT}\right)$	$K_3 = 5.4E2 \times \exp\left(-\frac{18.4}{RT}\right)$
$K_O = 1.5E\text{-}6 \times \exp\left(\frac{17.8}{RT}\right)$ Pa^{-1}	$K_O = 1.2E\text{-}7 \times \exp\left(\frac{28.9}{RT}\right)$ Pa^{-1}	$K_O = 8.1E\text{-}8 \times \exp\left(\frac{34.0}{RT}\right)$ Pa^{-1}	$K_O = 7.5E\text{-}7 \times \exp\left(\frac{32.9}{RT}\right)$ Pa^{-1}	$K_O = 1.2E\text{-}7 \times \exp\left(\frac{33.9}{RT}\right)$ Pa^{-1}	$K_O = 2.0E\text{-}6 \times \exp\left(\frac{20.1}{RT}\right)$ Pa^{-1}
$K_5 = 1.4E2 \times \exp\left(-\frac{35.5}{RT}\right)$	$K_5 = 2.3E1 \times \exp\left(-\frac{26.7}{RT}\right)$	$K_5 = 1.4E1 \times \exp\left(-\frac{25.9}{RT}\right)$	$K_5 = 1.2E1 \times \exp\left(-\frac{26.9}{RT}\right)$	$K_5 = 6.9E0 \times \exp\left(-\frac{26.7}{RT}\right)$	$K_5 = 1.5E2 \times \exp\left(-\frac{34.7}{RT}\right)$
$K_6 = 6.7E2 \times \exp\left(-\frac{22.9}{RT}\right)$	$K_6 = 3.0E1 \times \exp\left(-\frac{25.9}{RT}\right)$	$K_6 = 1.3E1 \times \exp\left(-\frac{27.8}{RT}\right)$	$K_6 = 3.4E0 \times \exp\left(-\frac{29.7}{RT}\right)$	$K_6 = 9.0E0 \times \exp\left(-\frac{27.2}{RT}\right)$	$K_6 = 5.5E2 \times \exp\left(-\frac{23.7}{RT}\right)$
$K_{DM} = 1.3E\text{-}6 \times \exp\left(\frac{17.4}{RT}\right)$ Pa^{-1}	$K_{DM} = 2.8E\text{-}8 \times \exp\left(\frac{25.6}{RT}\right)$ Pa^{-1}	$K_{DM} = 6.3E\text{-}8 \times \exp\left(\frac{27.4}{RT}\right)$ Pa^{-1}	$K_{DM} = 3.5E\text{-}7 \times \exp\left(\frac{29.8}{RT}\right)$ Pa^{-1}	$K_{DM} = 9.1E\text{-}8 \times \exp\left(\frac{26.9}{RT}\right)$ Pa^{-1}	$K_{DM} = 6.7E\text{-}7 \times \exp\left(\frac{15.7}{RT}\right)$ Pa^{-1}
$K_{DL} = 5.3E\text{-}3 \times \exp\left(\frac{4.6}{RT}\right)$ Pa^{-1}	$K_{DL} = 2.0E\text{-}5 \times \exp\left(\frac{39.6}{RT}\right)$ Pa^{-1}	$K_{DL} = 9.6E\text{-}6 \times \exp\left(\frac{36.6}{RT}\right)$ Pa^{-1}	$K_{DL} = 5.5E\text{-}6 \times \exp\left(\frac{33.2}{RT}\right)$ Pa^{-1}	$K_{DL} = 4.6E\text{-}6 \times \exp\left(\frac{36.7}{RT}\right)$ Pa^{-1}	$K_{DL} = 3.8E\text{-}3 \times \exp\left(\frac{4.5}{RT}\right)$ Pa^{-1}
$K_{AM} = 2.8E\text{-}18 \times \exp\left(\frac{2.0}{RT}\right)$ Pa^{-1}	$K_{AM} = 5.2E\text{-}10 \times \exp\left(\frac{4.3}{RT}\right)$ Pa^{-1}	$K_{AM} = 4.5E\text{-}10 \times \exp\left(\frac{4.3}{RT}\right)$ Pa^{-1}	$K_{AM} = 5.1E\text{-}10 \times \exp\left(\frac{4.4}{RT}\right)$ Pa^{-1}	$K_{AM} = 4.5E\text{-}10 \times \exp\left(\frac{4.3}{RT}\right)$ Pa^{-1}	$K_{AM} = 2.8E\text{-}18 \times \exp\left(\frac{2.0}{RT}\right)$ Pa^{-1}
$K_{AL} = 9.4E\text{-}2 \times \exp\left(\frac{7.2}{RT}\right)$ Pa^{-1}	$K_{AL} = 2.7E\text{-}1 \times \exp\left(\frac{6.1}{RT}\right)$ Pa^{-1}	$K_{AL} = 8.7E\text{-}1 \times \exp\left(\frac{8.2}{RT}\right)$ Pa^{-1}	$K_{AL} = 3.7E\text{-}1 \times \exp\left(\frac{7.0}{RT}\right)$ Pa^{-1}	$K_{AL} = 8.6E\text{-}1 \times \exp\left(\frac{8.2}{RT}\right)$ Pa^{-1}	$K_{AL} = 2.2E\text{-}1 \times \exp\left(\frac{7.8}{RT}\right)$ Pa^{-1}
$K_H = 5.8E\text{-}6 \times \exp\left(\frac{31.9}{RT}\right)$ Pa^{-1}	$K_H = 1.8E\text{-}7 \times \exp\left(\frac{39.7}{RT}\right)$ Pa^{-1}	$K_H = 4.8E\text{-}8 \times \exp\left(\frac{33.9}{RT}\right)$ Pa^{-1}	$K_H = 6.6E\text{-}9 \times \exp\left(\frac{34.3}{RT}\right)$ Pa^{-1}	$K_H = 2.1E\text{-}8 \times \exp\left(\frac{32.9}{RT}\right)$ Pa^{-1}	$K_H = 1.5E\text{-}5 \times \exp\left(\frac{34.1}{RT}\right)$ Pa^{-1}
$k'_P = 6.0E2 \times \exp\left(-\frac{50.7}{RT}\right)$ $mol \cdot s^{-1} \cdot kg_{cat}^{-1}$	$k'_P = 6.2E3 \times \exp\left(-\frac{41.8}{RT}\right)$ $mol \cdot s^{-1} \cdot kg_{cat}^{-1}$	$k'_P = 3.4E3 \times \exp\left(-\frac{40.6}{RT}\right)$ $mol \cdot s^{-1} \cdot kg_{cat}^{-1}$	$k'_P = 6.7E3 \times \exp\left(-\frac{44.3}{RT}\right)$ $mol \cdot s^{-1} \cdot kg_{cat}^{-1}$	$k'_P = 1.8E3 \times \exp\left(-\frac{42.1}{RT}\right)$ $mol \cdot s^{-1} \cdot kg_{cat}^{-1}$	$k'_P = 4.3E3 \times \exp\left(-\frac{36.7}{RT}\right)$ $mol \cdot s^{-1} \cdot kg_{cat}^{-1}$
$k'_O = 1.3E2 \times \exp\left(-\frac{8.4}{RT}\right)$ $mol \cdot s^{-1} \cdot kg_{cat}^{-1}$	$k'_O = 8.0E2 \times \exp\left(-\frac{11.4}{RT}\right)$ $mol \cdot s^{-1} \cdot kg_{cat}^{-1}$	$k'_O = 6.6E2 \times \exp\left(-\frac{11.4}{RT}\right)$ $mol \cdot s^{-1} \cdot kg_{cat}^{-1}$	$k'_O = 2.8E1 \times \exp\left(-\frac{18.7}{RT}\right)$ $mol \cdot s^{-1} \cdot kg_{cat}^{-1}$	$k'_O = 5.4E2 \times \exp\left(-\frac{12.1}{RT}\right)$ $mol \cdot s^{-1} \cdot kg_{cat}^{-1}$	$k'_O = 5.7E2 \times \exp\left(-\frac{6.0}{RT}\right)$ $mol \cdot s^{-1} \cdot kg_{cat}^{-1}$
$k'_{DM} = 1.1E3 \times \exp\left(-\frac{6.4}{RT}\right)$ $mol \cdot s^{-1} \cdot kg_{cat}^{-1}$	$k'_{DM} = 2.3E\text{-}7 \times \exp\left(-\frac{82.7}{RT}\right)$ $mol \cdot s^{-1} \cdot kg_{cat}^{-1}$	$k'_{DM} = 2.2E\text{-}7 \times \exp\left(-\frac{82.7}{RT}\right)$ $mol \cdot s^{-1} \cdot kg_{cat}^{-1}$	$k'_{DM} = 2.2E\text{-}7 \times \exp\left(-\frac{82.7}{RT}\right)$ $mol \cdot s^{-1} \cdot kg_{cat}^{-1}$	$k'_{DM} = 2.2E\text{-}7 \times \exp\left(-\frac{82.7}{RT}\right)$ $mol \cdot s^{-1} \cdot kg_{cat}^{-1}$	$k'_{DM} = 6.9E2 \times \exp\left(-\frac{7.1}{RT}\right)$ $mol \cdot s^{-1} \cdot kg_{cat}^{-1}$
$k'_{DL} = 3.6E5 \times \exp\left(-\frac{4.2}{RT}\right)$ $mol \cdot s^{-1} \cdot kg_{cat}^{-1}$	$k'_{DL} = 1.9E4 \times \exp\left(-\frac{6.9}{RT}\right)$ $mol \cdot s^{-1} \cdot kg_{cat}^{-1}$	$k'_{DL} = 1.4E4 \times \exp\left(-\frac{7.3}{RT}\right)$ $mol \cdot s^{-1} \cdot kg_{cat}^{-1}$	$k'_{DL} = 4.2E3 \times \exp\left(-\frac{7.2}{RT}\right)$ $mol \cdot s^{-1} \cdot kg_{cat}^{-1}$	$k'_{DL} = 1.0E4 \times \exp\left(-\frac{7.6}{RT}\right)$ $mol \cdot s^{-1} \cdot kg_{cat}^{-1}$	$k'_{DL} = 1.0E7 \times \exp\left(-\frac{3.6}{RT}\right)$ $mol \cdot s^{-1} \cdot kg_{cat}^{-1}$

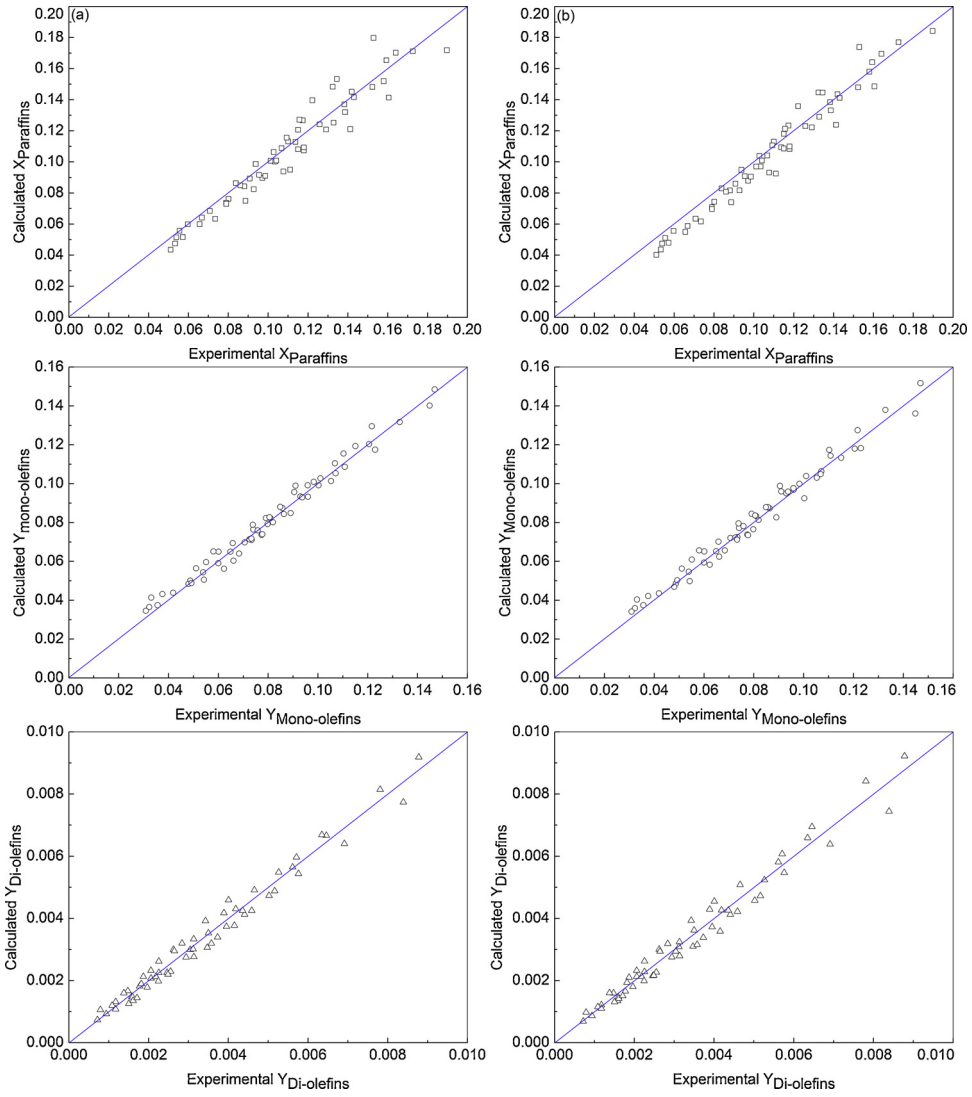

Fig. 4. Fitting results of Model 4 (a) and Model 5 (b) *versus* experimental results.

pathway only involves the reaction on Pt sites (Reaction No. 8, Table 1). The estimated kinetic parameters in Table 4, along with the simulation results, indicate that the former pathway is predominant. Thus, the above calculations prove the reported assumption that aromatization and further coking are accelerated by acid sites together with Pt sites [2]. Because highly dispersed metal (Pt) sites are required for high reaction rates for long chain paraffin dehydrogenation to olefins, neutralization of the Lewis acid sites is expected to lower aromatics and coke formation rates for improved olefin selectivity and prolonged catalyst lifetime. Indeed, this is done in practice by modifying the catalysts with alkali metals such as Li [7,8], Na [45], K [6,7] and Cs [45].

5. Conclusions

The empirical model presented here for the kinetics of *n*-dodecane dehydrogenation over the Pt-Sn-K-Mg/γ-Al_2O_3 catalyst shows promise by successfully predicting the yields of mono- and di-olefins within the industrially relevant conditions (450–470 °C, 0.17 − 0.30 MPa, H_2/paraffin mole ratios between 3:1 and 6:1, space times between 0.22–1.57 g h mol^{-1}). Operation at low space time, high pressure, high H_2/paraffin ratio and low reaction temperature is favorable to high mono-olefins selectivity. The bi-functional model is relevant because it is based on the elementary reactions on Pt and Lewis acid sites, key characteristics of this dehydrogenation catalyst. Within the six reaction rate models tested, the surface step involving the interaction of Pt-H and Pt-alkyl species to result in an absorbed mono-olefin or di-olefin is observed to be the kinetically relevant rate determining step. The kinetic modeling indicates that the increased temperature within a certain range (*e.g.*, 450–490 °C) has little effect on mono-olefin selectivity, which opens the opportunity for the industry to maintain the productivity at later period of catalyst life-time by increasing the operation temperature while keeping relatively stable product selectivity. Kinetic data also suggests that aromatization was majorly caused by Pt and Lewis acid sites in a concerted way. This is critical in the design of an efficient catalyst as, lowering the aromatics formation by neutralizing Lewis acid sites can (i) improve olefin selectivity and (ii) prolong catalyst life-time as aromatics are precursor to coke. Both are extremely relevant of commercial operation of long chain paraffins dehydrogenation catalysts.

Acknowledgments

Financial support from the Liaoning Provincial Natural Science Foundation of China (Grant No. 2013020111) and a visiting professor program from the King Saud University, Saudi Arabia for this research are acknowledged. S. He also thanks Prof. C. Sun at Dalian Institute of Chemical Physics, Chinese Academy of Sciences for collaborations on R

&D and commercialization activities regarding paraffin dehydrogenation and Y. Lai for his assistance on kinetic measurements.

Appendix A. Supplementary data

Supplementary material related to this article can be found, in the online version, at doi:https://doi.org/10.1016/j.apcata.2019.04.026.

References

[1] S. He, Chemical Engineering, Dalian Institute of Chemical Physics, Chinese Academy of Sciences, Dalian, 2009, pp. 1–198.
[2] M.M. Bhasin, J.H. McCain, B.V. Vora, T. Imai, P.R. Pujado, Applied Catalysis a-General. 221 (2001) 397–419.
[3] B.V. Vora, Top. Catal. 55 (2012) 1297–1308.
[4] S. He, H. Cui, Y. Lai, C. Sun, S. Luo, H. Li, K. Seshan, Catal. Sci. Technol. 5 (2015) 4959–4963.
[5] S. He, D. Chen, H. Cui, Y. Lai, C. Sun, H. Li, A.S. Al-Fatesh, I.A. Aidid, A.H. Fakeeha, K. Seshan, Appl. Catal. A Gen. 514 (2016) 241–247.
[6] S. He, Y. Lai, W. Bi, X. Yang, X. Rong, C. Sun, Chinese J. Catal. 31 (2010) 435–440.
[7] A.D. Qiu, Y.N. Fan, Y.F. Ma, P.C. Wu, Y. Chen, Chinese J. Catal. 22 (2001) 343–347.
[8] D.T. Gokak, A.G. Basrur, D. Rajeswar, G.S. Rao, K.R. Krishnamurthy, React. Kinet. Catal. Lett. 59 (1996) 315–323.
[9] Y. Lai, S. He, X. Li, C. Sun, K. Seshan, Applied Catalysis a-General. 469 (2014) 74–80.
[10] Y. Lai, S. He, S. Luo, W. Bi, X. Li, C. Sun, K. Seshan, Catal. Commun. 69 (2015) 39–42.
[11] O.B. Belskaya, L.N. Stepanova, T.I. Gulyaeva, D.V. Golinskii, A.S. Belyi, V.A. Likholobov, Kinet. Catal. 56 (2015) 655–662.
[12] A.A. Castro, Catal. Letters 22 (1993) 123–133.
[13] A.P. Barkova, D.B. Furman, Kinet. Catal. 35 (1994) 861–864.
[14] A.D. Ballarini, S.R. de Miguel, A.A. Castro, O.A. Scelza, Applied Catalysis a-General 467 (2013) 235–245.
[15] X. Li, S. He, H. Wei, S. Luo, B. Gu, C. Sun, Russ. J. Phys. Chem. 89 (2015) 1368–1373.
[16] S. Luo, S. He, X. Li, C. Sun, K. Seshan, Catal. Today 234 (2014) 295–300.
[17] S. He, C. Sun, H. Du, X. Dai, B. Wang, Chem. Eng. J. 141 (2008) 284–289.
[18] S. He, B. Wang, X. Dai, C. Sun, Z. Bai, X. Wang, Q. Guo, Chem. Eng. J. 275 (2015) 298–304.
[19] T.L. Krylova, N.V. Nekrasov, B.S. Gudkov, V.R. Gurevich, S.L. Kiperman, Kinet. Catal. 21 (1980) 1060–1063.
[20] Z.A. Sadykhova, N.V. Nekrasov, V.R. Gurevich, S.L. Kiperman, Kinet. Catal. 22 (1981) 303–308.
[21] Z.A. Sadykhova, N.V. Nekrasov, V.R. Gurevich, S.L. Kiperman, Kinet. Catal. 25 (1984) 497–501.
[22] A.G. Basrur, D. Rajeshwer, D.T. Gokak, G.S. Rao, K.R. Krishnamurthy, T. Rao, G. Dhar (Eds.), Studies in Surface Science and Catalysis, 1998, pp. 809–814.
[23] G. Padmavathi, K.K. Chaudhuri, D. Rajeshwer, G.S. Rao, K.R. Krishnamurthy, P.C. Trivedi, K.K. Hathi, N. Subramanyam, Chem. Eng. Sci. 60 (2005) 4119–4129.
[24] L. Vafajoo, F. Khorasheh, M.H. Nakhjavani, M. Fattahi, Pet. Sci. Technol. 32 (2014) 813–820.
[25] E.N. Ivashkina, E.V. Frantsina, R.V. Romanovsky, I.M. Dolganov, E.D. Ivanchina, A.V. Kravtsov, Catal. Ind. 4 (2012) 110–120.
[26] N.A. Gaidai, S.L. Kiperman, Kinet. Catal. 42 (2001) 527–532.
[27] M. Saeedizad, S. Sahebdelfar, Z. Mansourpour, Chem. Eng. J. 154 (2009) 76–81.
[28] S. Luo, S. He, X. Li, J. Li, W. Bi, C. Sun, Fuel Process. Technol. 129 (2015) 156–161.
[29] S. He, K.R. Krishnamurthy, K. Seshan, Catalysis: Volume 29, The Royal Society of Chemistry, 2017, pp. 282–316.
[30] J.J.H.B. Sattler, J. Ruiz-Martinez, E. Santillan-Jimenez, B.M. Weckhuysen, Chem. Rev. 114 (2014) 10613–10653.
[31] S. Brunauer, P.H. Emmett, E. Teller, J. Am. Chem. Soc. 60 (1938) 309–319.
[32] E.P. Barrett, L.G. Joyner, P.P. Halenda, J. Am. Chem. Soc. 73 (1951) 373–380.
[33] A. Le Valant, C. Comminges, F. Can, K. Thomas, M. Houalla, F. Epron, J. Phys. Chem. C 120 (2016) 26374–26385.
[34] S. He, C. Sun, Z. Bai, X. Dai, B. Wang, Applied Catalysis a-General 356 (2009) 88–98.
[35] C.D. Prater, Chem. Eng. Sci. 8 (1958) 284–286.
[36] O. Levenspiel, Chemical Reaction Engineering, 3rd ed., John Wiley & Sons, New York, 1999.
[37] B.V. Vora, P.R. Pujado, Encyclopedia of Chemical Processing, Taylor & Francis Group, New York, 2006.
[38] J.C. Afonso, M. Schmal, R. Frety, Fuel Process. Technol. 41 (1994) 13–25.
[39] S.K. Sahoo, P.V.C. Rao, D. Rajeshwer, K.R. Krishnamurthy, I.D. Singh, Applied Catalysis a-General 244 (2003) 311–321.
[40] K.S.W. Sing, D.H. Everett, R.A.W. Haul, L. Moscou, R.A. Pierotti, J. Rouquerol, T. Siemieniewska, Pure Appl. Chem. 57 (1985) 603–619.
[41] B. Kang, H. Tang, G. Zhang, Y. Lu, China Surfactant Detergent & Cosmetics (1986) 1–6.
[42] H. Jiang, S. Ren, L. Zhou, Y. Wang, J. Cao, Pet. Sci. Technol. 33 (2015) 1305–1313.
[43] A.P. Tyupaev, E.A. Timofeeva, G.V. Isagulyants, Bull. Acad. Sci. Ussr Div. Chem. Sci. 34 (1985) 182–185.
[44] M. Akia, S.M. Alavi, Z.-F. Yan, Petroleum & Coal 52 (2010) 280–289.
[45] E.A. Timofeeva, A.P. Tyupaev, G.V. Isagulyants, Bull. Acad. Sci. Ussr Div. Chem. Sci. 31 (1982) 2347–2350.